Supporting Information for

Exciton-Phonon Coupling and Power Dependent Room Temperature Photoluminescence of Sulphur Vacancy Doped MoS_2 via Controlled Thermal Annealing

Dario Mastrippolito,[a] Stefano Palleschi,[a] Gianluca D'Olimpio,[a] Antonio Politano,[a,b] Michele Nardone,[a] Paola Benassi[a] and Luca Ottaviano[a,c,*]

[a] Dipartimento di Scienze Fisiche e Chimiche (DSFC), Università dell'Aquila, Via Vetoio 10 67100 L'Aquila, Italy

[b] CNR-IMM Istituto per la Microelettronica e Microsistemi, VIII strada 5 Catania I-95121, Italy

[c] CNR-SPIN UOS L'Aquila, Via Vetoio 10 67100 L'Aquila, Italy

[*] E-mail: luca.ottaviano@aquila.infn.it

1 AFM analysis

From AFM images of MoS_2 flakes acquired after the annealing process, we observed the formation of etch pits on the surfaces of few layer and bulk MoS_2. In figure 1 we show the comparison between some images belonging to the same MoS_2 flakes, before and after annealing. Pits were observed by various studies[1–4] and by our previous findings.[5] The pits shape is crucial for understanding their origin, as indicated by Yamamoto et al.[1]. In particular, triangular pits are attributable to anisotropic oxidation phenomena, and their lateral size and depth can increase with annealing time, evolving their shape and becoming hexagonal/circular pits.[6,7]

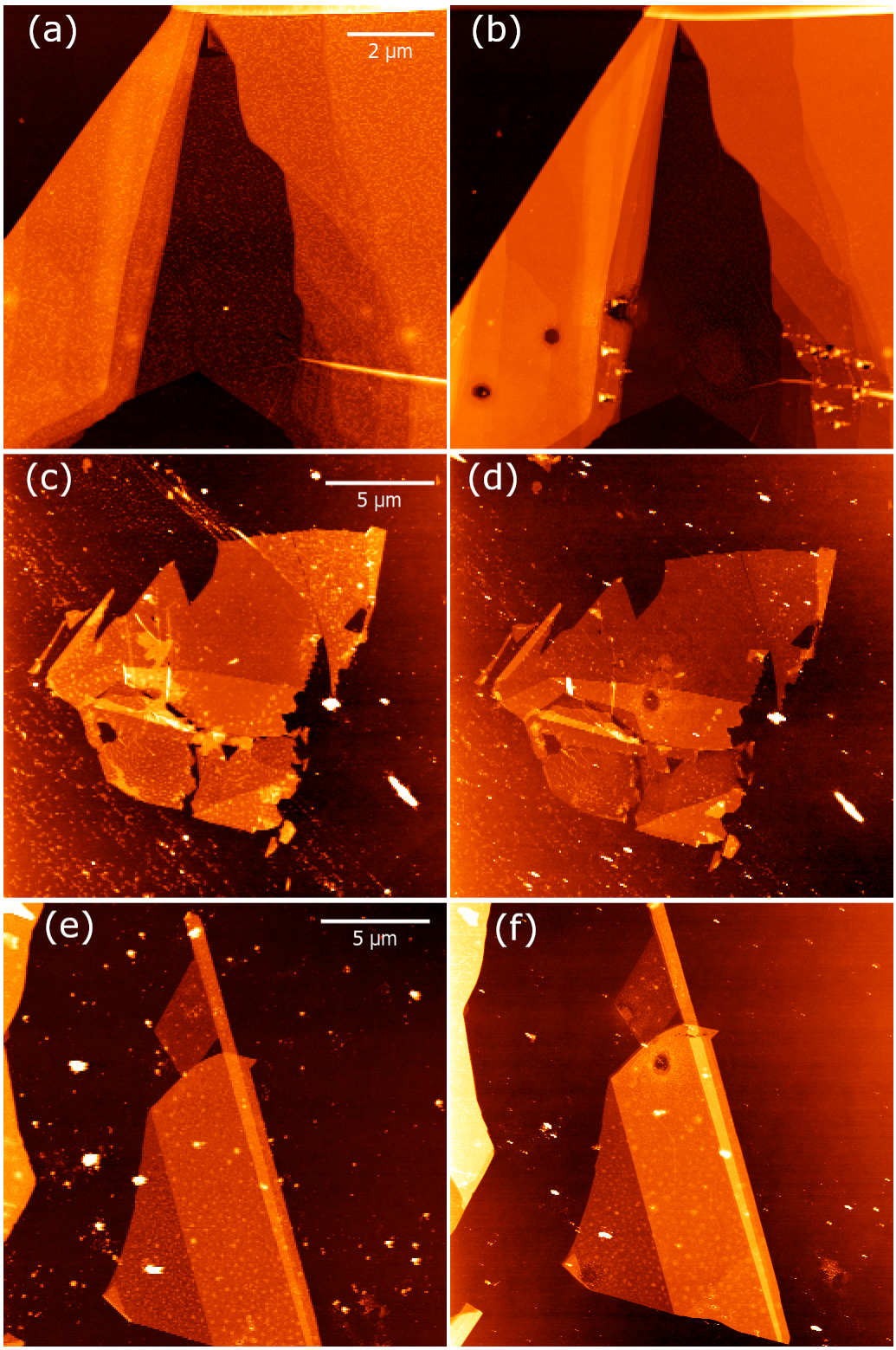

Figure 1 As-exfoliated and annealed AFM images of few layer MoS_2 flakes on 270 nm SiO_2/Si (100). (a) as-exfoliated flakes. (b) same flakes from (a) after annealing in air at 250 ℃ for 1 hour. (c) as-exfoliated flakes. (d) same flakes from (c) after annealing in air at 262.5 ℃ for 1 hour. (e) as-exfoliated flakes. (f) same flakes from (e) after annealing in air at 275 ℃ for 1 hour.

The thickness measurements of single layer MoS_2 with AFM show a generalized thinning of the flakes after the annealing process at any temperature. In table 1 we report the height distances of the mono-layers from the substrate, before and after the annealing, and their height differences. The decrease in the height measurements of the MoS_2 mono-layers is due to the removal, because of the high temperatures, of any impurities, contaminants and organic residues that may be present on the MoS_2 flakes deriving the production process.[8] Another explanation is due to the evaporation of water which could be present both under the flakes, at the interface between MoS_2 and the SiO_2/Si substrate,[9] and above the flakes, in different quantities than that present on the substrate due to the different hydrophilic and hydrophobic properties of the two materials, MoS_2 and SiO_2. In figure 2 we show that there is no correlation between the lowering of the distance from the substrate due to annealing process and the annealing temperature.

Table 1 mono-layers MoS_2 distances from SiO_2/Si substrate

Annealing Temperature (°C)	Height Before Annealing (nm)	Height After Annealing (nm)	Height Difference (nm)
200.0	4.0	1.9	2.1
212.5	3.8	2.5	1.3
225.0	4.2	2.6	1.6
237.5	2.9	1.8	1.1
250.0	2.9	2.0	0.9
262.5	3.6	1.4	2.2
275.0	3.1	1.3	1.8
287.5	3.6	1.4	2.2
300.0	3.7	2.4	1.3

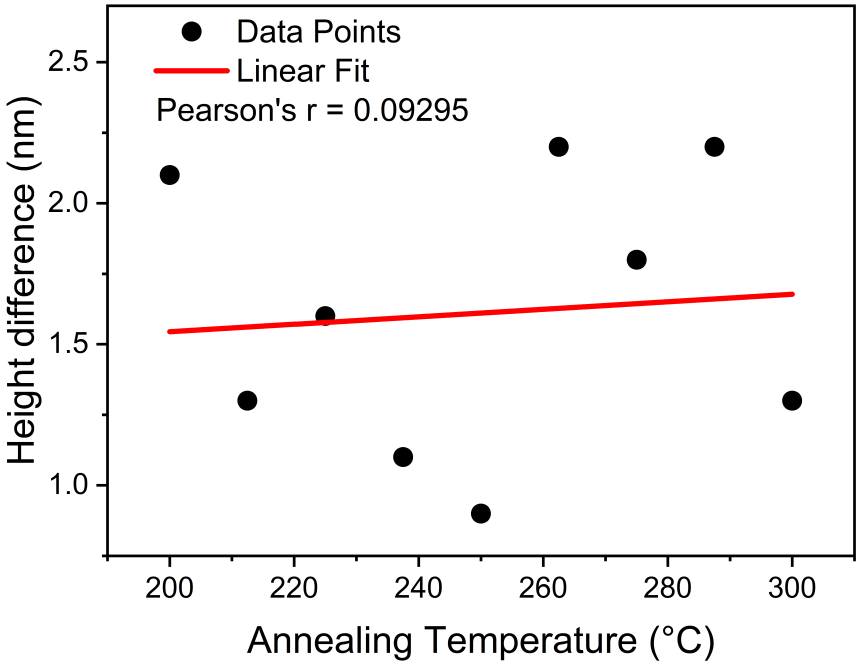

Figure 2 1L MoS_2 height differences after annealing processes. Height difference values from table 1 are plotted as functions of annealing temperature. The red line shows the linear fit of data points.

2 Power dependent PL analysis

In PL spectra of single-layer MoS_2 grown by *Chemical Vapor Deposition* (CVD) it seems to be possible to detect a C type exciton related peak centred at $\sim$ 700 nm, as evidenced by Kaplan studies[10,11]. This C band is due to a bound exciton with a binding energy of $\sim$ 55 meV, presumably due to an unintentional impurity or a native point defect, as reported by Kaplan et al.[10]. A comparison between our and Kaplan PL spectra is shown in figure 3. The Kaplan PL spectrum was digitalized from reference[10] and normalized for comparison.

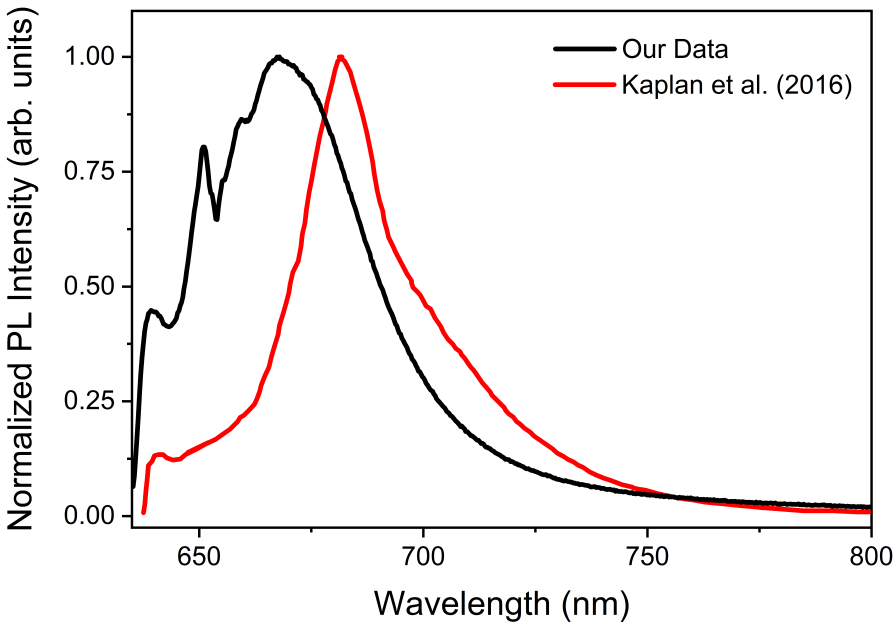

Figure 3 Normalized PL spectra of MoS_2 mono-layers produced by mechanical exfoliation and CVD. Normalized PL spectra of mechanical exfoliated MoS_2 mono-layer from our experiment (black line) and normalized PL spectra of MoS_2 mono-layer grown by CVD form Kaplan et al.[10]. Both samples have the same SiO_2/Si substrate and both spectra were acquired at room temperature with same excitation laser wavelength λ = 632.8 nm and comparable laser power range of 1 mW.

In PL spectra from mechanically/chemically exfoliated MoS_2 mono-layer like ours, this C type exciton related peak does not seem to be present in various studies[2,12–16] and our previous findings.[5] The interpretation of the PL signal composed of A and C types excitons is also not in agreement with our fit results. We tried to consider a PL spectral component around 700 nm getting no improvements in terms of R^2 value. Furthermore we also exclude the possibility that the A^- peak related to trion can be interpreted as C type exciton related peak, since the binding energy of the C exciton ($\sim$ 55 meV[10]) are too high compared to the mean binding energy of A^- trion ($\sim$ 29 meV) obtained by our fit, which is in agreement our previous analysis.[5]

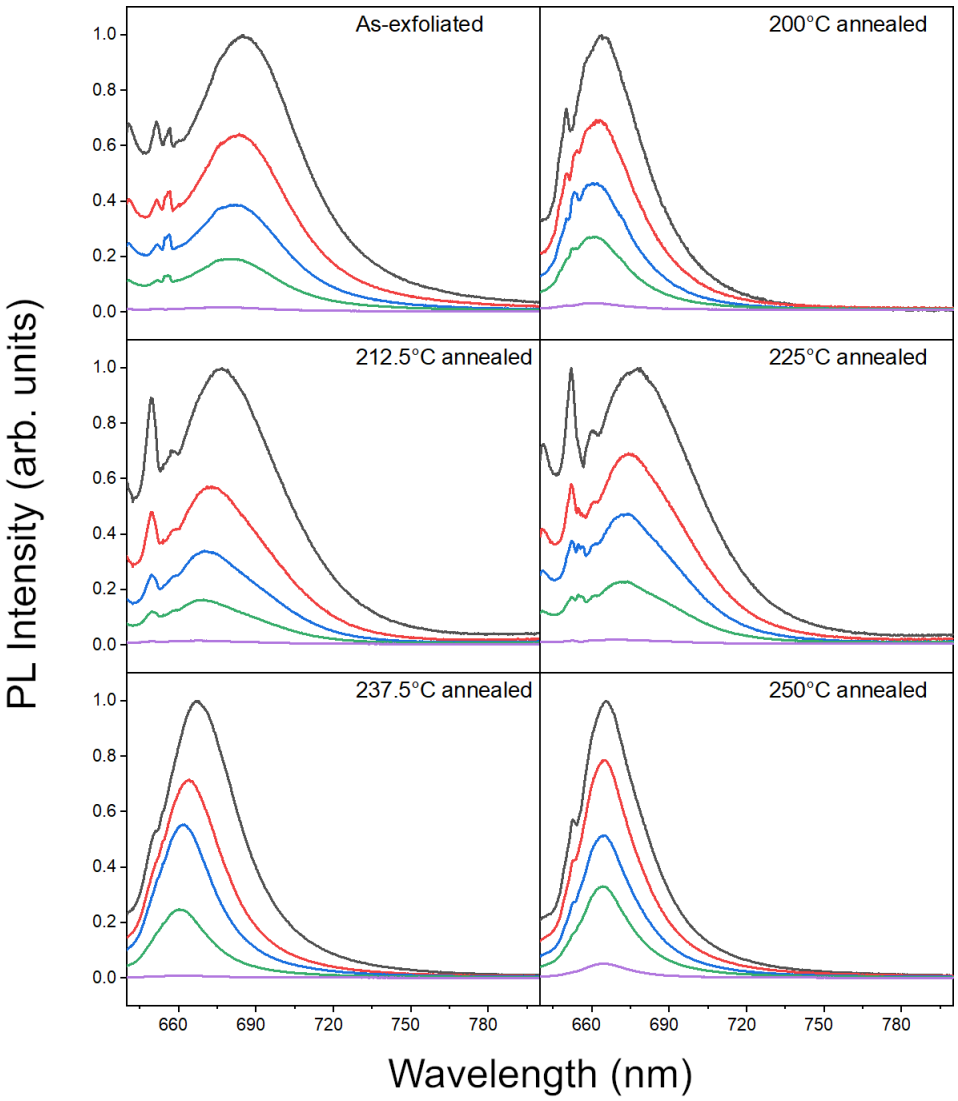

Figure 4 Continue

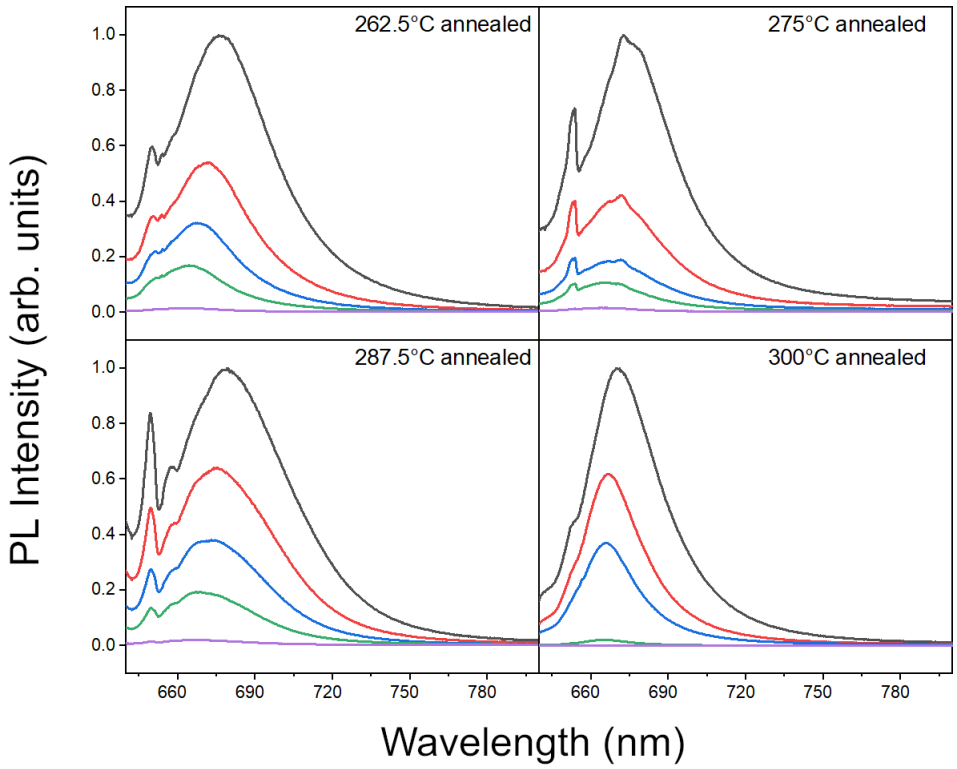

Figure 5 Normalized PL spectra of 1L MoS_2 on 270 nm SiO_2/Si (100) acquired at different laser powers (1.00 mW (black line), 0.50 mW (red line), 0.25 mW (blue line), 0.10 mW (green line), 0.01 mW (violet line)). PL spectra have been normalized to the maximum count measured at 1.00 mW laser power

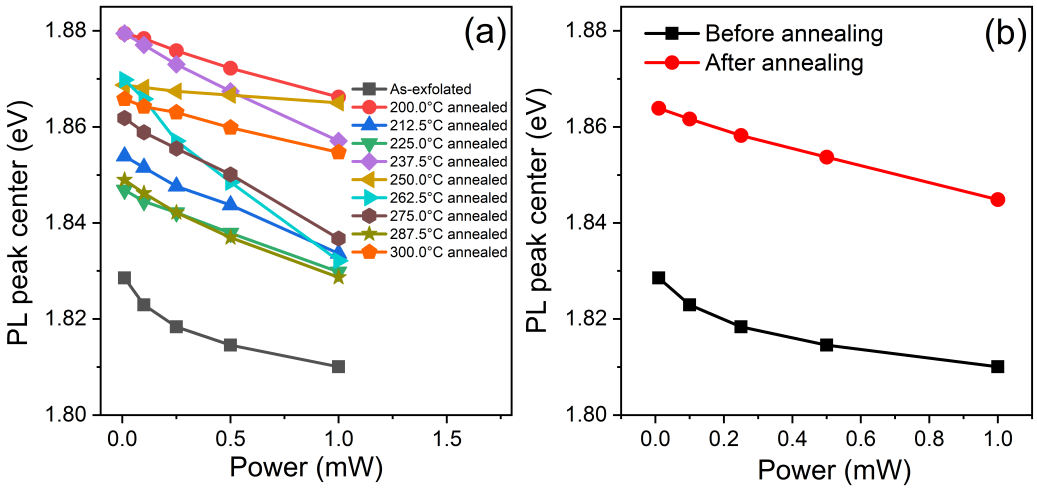

Figure 6 PL peak positions as functions of laser power. (a) PL peak positions of annealed samples (coloured) and mean PL peak position of as-exfoliated samples (black) are plotted as functions of laser power. (b) Mean PL peak position of annealed samples from (a) and mean PL peak position of as-exfoliated samples are plotted as functions of laser power.

Table 2 Mean position and mean FWHM of A^0 and A^- fitted peaks. PL spectra of annealed samples have been fitted with two Lorentzian line shapes and the mean position and mean FWHM of A^0 and A^- fitted peaks at different laser powers are reported.

Power (mW)	A^0 position (nm | eV)	A^0 FWHM (nm)	A^- position (nm | eV)	A^- FWHM (nm)
1.00	665.3 | 1.864	33	675.8 | 1.835	35
0.50	662.2 | 1.872	27	674.1 | 1.839	32
0.25	661.0 | 1.876	25	672.0 | 1.845	30
0.10	660.5 | 1.877	22	670.7 | 1.849	30
0.01	660.3 | 1.878	20	670.0 | 1.850	27

Table 3 Fit parameters of the normalized PL intensity yield power laws. Normalized PL yields as functions of laser power were fitted with trial power function $I/I_0 = aP^b$, where P is the excitation laser power. The values of fit parameters are reported.

Annealing Temperature (°C)	a	b
200.0	1.00 ± 0.02	0.62 ± 0.03
212.5	1.00 ± 0.01	0.89 ± 0.01
225.0	1.00 ± 0.01	0.69 ± 0.01
237.5	1.00 ± 0.02	0.67 ± 0.03
250.0	1.01 ± 0.01	0.54 ± 0.03
262.5	0.99 ± 0.02	1.00 ± 0.04
275.0	0.99 ± 0.03	1.13 ± 0.06
287.5	1.00 ± 0.01	0.80 ± 0.02
300.0	1.01 ± 0.01	0.54 ± 0.03
Mean as-exfoliated	1.00 ± 0.01	0.77 ± 0.01
Mean after annealing	1.00 ± 0.02	0.76 ± 0.03

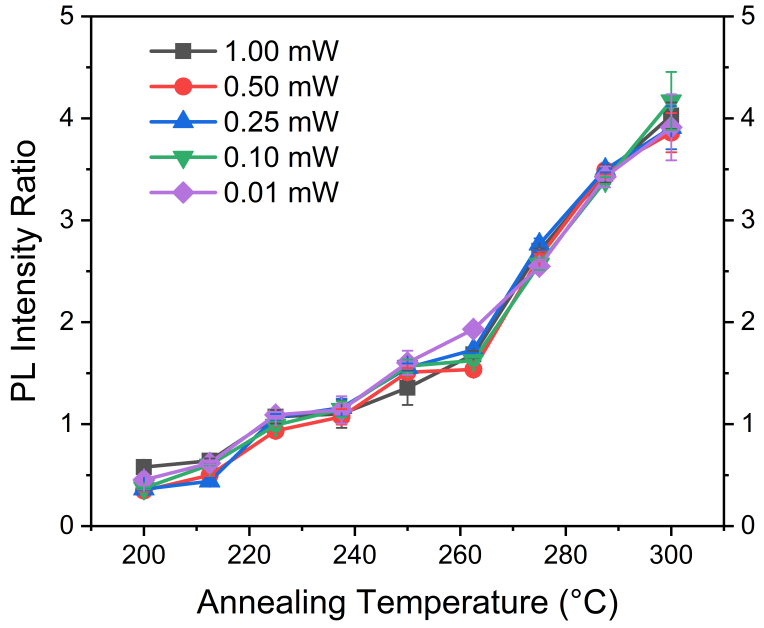

Figure 7 PL Intensity Ratio of annealed samples acquired at different laser powers are plotted as functions of annealing temperature.

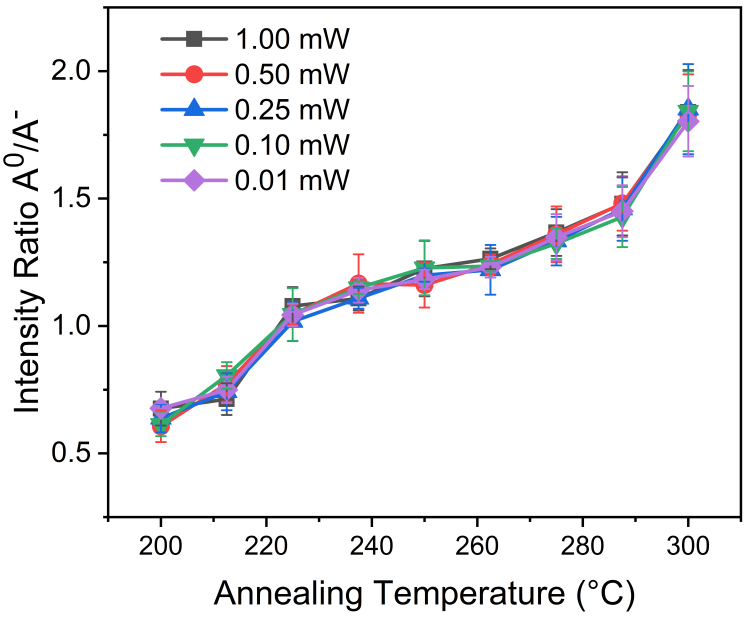

Figure 8 Ratio of the PL intensities of the A^0 and A^- fitted peaks of annealed samples PL spectra acquired at different laser powers are plotted as functions of annealing temperature.

From Figure 9 (a) the PL intensities ratio between A^0 and A^- fitted peaks (labelled as $\frac{I_{A^0}}{I_{A^-}}$) shows a slight increase for high laser powers for annealed samples at temperatures greater than or equal to 225 °C. This behaviour is also found in the PL spectral weight of A^0 (labelled as $\frac{I_{A^0}}{I_{total}}$) in Figure 9 (c) and consequently a slight decrease for high laser powers is present in the PL spectral weight of A^- (labelled as $\frac{I_{A^-}}{I_{total}}$) in Figure 9 (b). Therefore we quantified these increases of $\frac{I_{A^0}}{I_{A^-}}$ and $\frac{I_{A^0}}{I_{total}}$ considering only the annealed samples at temperature greater than or equal to 225 °C. To compare the values belonging to different temperatures annealing processes we normalized to the values acquired at maximum laser power and then averaged over the different annealing temperatures. The results are shown in the figure 10. These results suggest that the PL intensities ratio between A^0 and A^- peaks and the PL spectral weights of A^0 and A^- peaks are slightly influenced by the excitation laser power.

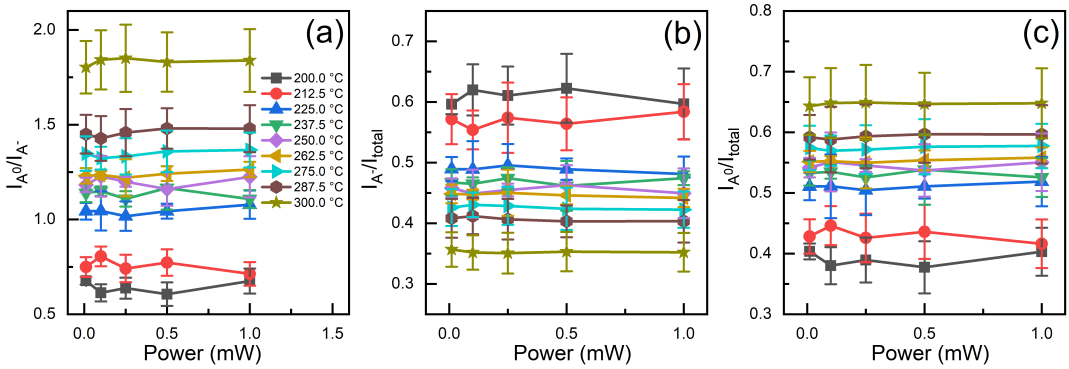

Figure 9 (a) Ratios of the PL intensities of the A^0 and A^- fitted peaks of annealed samples are plotted as functions of excitation laser power. (b) PL spectral weights of A^- fitted peak of annealed samples are plotted as functions of excitation laser power. (c) PL spectral weights of A^0 fitted peak of annealed samples are plotted as functions of excitation laser power.

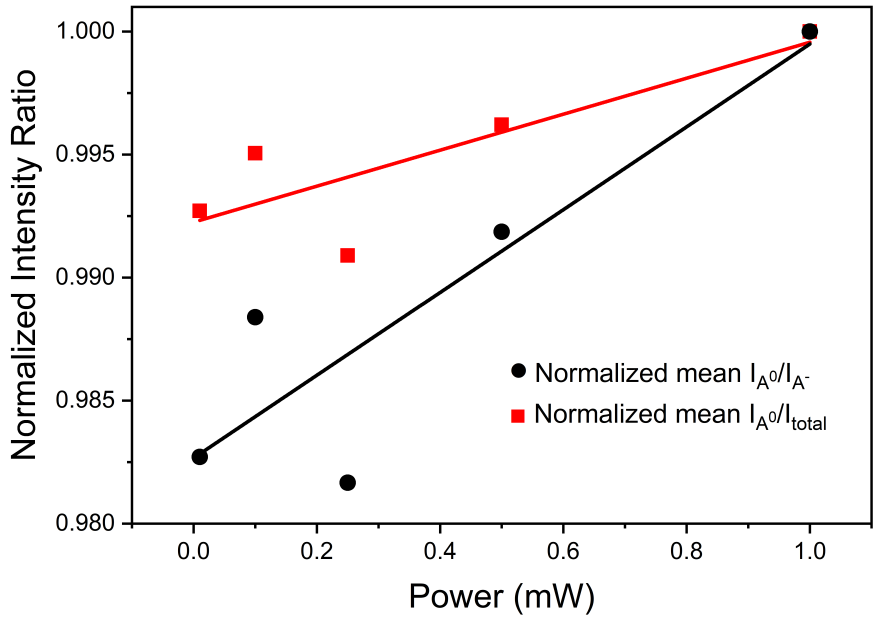

Figure 10 Normalized mean ratio of the PL intensities of the A^0 and A^- fitted peaks (black) and normalized mean PL intensity weight of A^0 fitted peak (red) are plotted as functions of laser power. They have been normalized to the maximum respective values obtained at 1.00 mW laser power then they were averaged over the annealing temperatures between 225 ℃ and 300 ℃.

3 Resonant Raman Analysis

Table 4 Mean position and mean FWHM of Raman fitted peaks

	Position as-exfoliated (cm^{-1})	Position after annealing (cm^{-1})	FWMH as-exfoliated (cm^{-1})	FWMH after annealing (cm^{-1})
E'(M)	378	377	10	9
E^1_{2g}	384	383	8	8
A_{1g}	405	404	9	8
$LA(\sim K)+TA(\sim K)$	417	417	18	17
$A_{1g}(\Gamma)+E^2_{2g}(\Gamma)$	436	438	18	15
2LA(vHs)	446	449	13	13
$2LA(\sim K)$	456	458	13	11
$2LA(\sim M)$	466	466	12	10

3.1 Oxygen adsorption evidences

We expect oxygen adsorption on the sulfur vacancies, generated due to the annealing processes. In the resonant Raman spectra of the MoS_2 samples, both before and after the annealing processes, there are no attributable peaks to chemical bonds between Mo and O, which would be a direct confirmation of the occurred oxygen adsorption. In Figure 11 shows the RT resonant Raman spectra acquired at 1.00 mW excitation laser power of a single-layer MoS_2 acquired before and after annealing in air at 300 °C for one hour and, by comparison, in the inset the Raman spectrum of MoO_3 powder taken from article[17] and obtained in almost compatible experimental conditions of our experiment (same excitation radiation λ = 632.8 nm (E = 1.96 eV), back-scattering configuration, RT and not very high laser power of 0.6 mW. In our previous work[18] MoO_3 was found on the surface of MoS_2 samples through XPS spectroscopy and gas sensing experiments but no peaks were detected in resonant Raman spectra of MoS_2. The absence of MoO_3 detection peaks in Raman spectra of single-layer and few-layer MoS_2 samples is noted by Kang et al.[19], after having detected the presence of MoO_3 through XPS spectroscopy on similarly treated samples.[19,20] This lack is justified by assuming that the structure of MoO_3 on MoS_2 has a slightly different symmetry than that of bulk MoO_3 due to interactions between Mo and S atoms. Moreover, as reported by various studies,[21–23] the Raman spectra of the single-layer and few-layer MoS_2 are significantly amplified by the effect of the interference and multiple reflections of the laser light that occurs in the layered structure $MoS_2/SiO_2/Si$. This amplification is lacking in the case of MoO_3 if present in small non-layered structures such as those that are formed at the sulphur vacancies on MoS_2. We have reason to say that this is the reason why the MoO_3 Raman peaks are not observed. However an indication of the occurred oxygen absorption comes from the position of the E^1_{2g} Raman peak of MoS_2. Indeed, as reported by Bera et al.[13], the softening of the E^1_{2g} Raman peak position, after the annealing (see table 4), is due precisely to the oxygen adsorption.

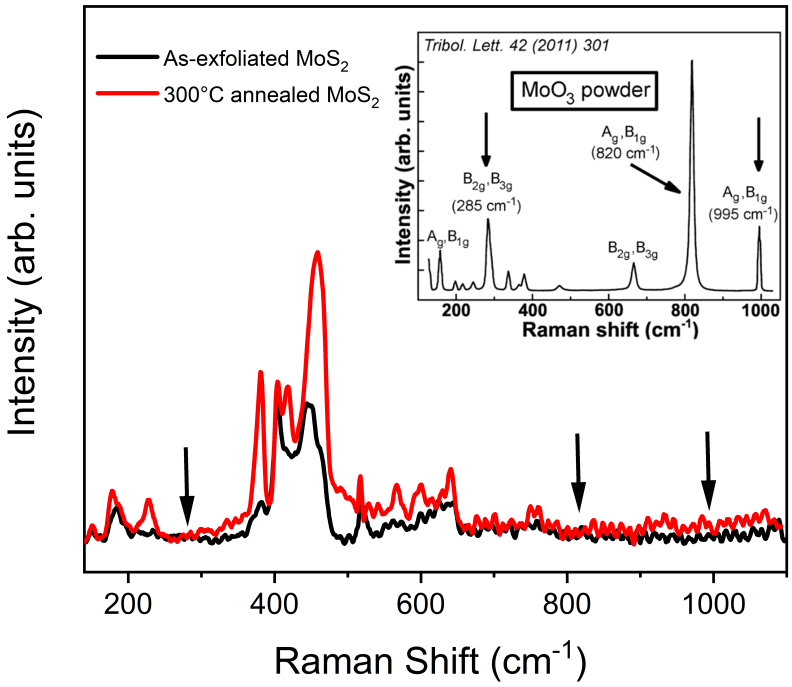

Figure 11 MoS_2 and MoO_3 powder Raman spectra. Main panel, Raman spectra of 1L MoS_2 on 270 nm SiO_2/Si (100), acquired at 1 mW laser power, in 140÷1100 cm^{-1} spectral region, as-exfoliated (black line) and after annealing (red line) in air at 300 ℃ for 1 hour. In the inset, Raman spectrum of MoO_3 powder from Windom et al.[17], three arrows in the main panel point to the peak positions of the most intense MoO_3 spectral features at 285 cm^{-1}, 820 cm^{-1} and 995 cm^{-1} assigned to (B_{2g}, B_{3g}), (A_g, B_{1g}), and (A_g, B_{1g}) modes respectively.

References

[1] M. Yamamoto, T. L. Einstein, M. S. Fuhrer and W. G. Cullen, *The Journal of Physical Chemistry C*, 2013, **117**, 25643–25649.

[2] X. Wang, W. Fan, Z. Fan, W. Dai, K. Zhu, S. Hong, Y. Sun, J. Wu and K. Liu, *Nanoscale*, 2018, **10**, 3540–3546.

[3] H. Nan, Z. Wang, W. Wang, Z. Liang, Y. Lu, Q. Chen, D. He, P. Tan, F. Miao, X. Wang, J. Wang and Z. Ni, *ACS Nano*, 2014, **8**, 5738–5745.

[4] J. Wu, H. Li, Z. Yin, H. Li, J. Liu, X. Cao, Q. Zhang and H. Zhang, *Small*, 2013, **9**, 3314–3319.

[5] S. Palleschi, G. D'Olimpio, P. Benassi, M. Nardone, R. Alfonsetti, G. Moccia, M. Renzelli, O. Cacioppo, A. Hichri, S. Jaziri, A. Politano and L. Ottaviano, *2D Materials*, 2020, **7**, 025001.

[6] Z. Wang, Q. Li, H. Xu, C. Dahl-Petersen, Q. Yang, D. Cheng, D. Cao, F. Besenbacher, J. V. Lauritsen, S. Helveg and D. Mingdong, *Nano Energy*, 2018, **49**, 634–643.

[7] A. Yoon, J. H. Kim, J. Yoon, Y. Lee and Z. Lee, *ACS Applied Materials & Interfaces*, 2020, **12**, 22029–22036.

[8] S. Tongay, J. Zhou, C. Ataca, J. Liu, J. S. Kang, T. S. Matthews, L. You, J. Li, J. C. Grossman and J. Wu, *Nano Letters*, 2013, **13**, 2831–2836.

[9] K. S. Novoselov, A. K. Geim, S. V. Morozov, D. Jiang, Y. Zhang, S. V. Dubonos, I. V. Grigorieva and A. A. Firsov, *Science*, 2004, **306**, 666–669.

[10] D. Kaplan, Y. Gong, K. Mills, V. Swaminathan, P. Ajayan, S. Shirodkar and E. Kaxiras, *2D Materials*, 2016, **3**, 015005.

[11] D. Kaplan, K. Mills, J. Lee, S. Torrel and V. Swaminathan, *Journal of Applied Physics*, 2016, **119**, 214301.

[12] P. J. Ko, A. Abderrahmane, T. V. Thu, D. Ortega, T. Takamura and A. Sandhu, *Journal of Nanoscience and Nanotechnology*, 2015, **15**, 6843–6846.

[13] A. Bera, D. Muthu and A. Sood, *Journal of Raman Spectroscopy*, 2018, **49**, 100–105.

[14] S. Mouri, Y. Miyauchi and K. Matsuda, *Nano Letters*, 2013, **13**, 5944–5948.

[15] S. Tongay, J. Zhou, C. Ataca, K. Lo, T. S. Matthews, J. Li, J. C. Grossman and J. Wu, *Nano Letters*, 2012, **12**, 5576–5580.

[16] X. Wei, Z. Yu, F. Hu, Y. Cheng, L. Yu, X. Wang, M. Xiao, J. Wang, X. Wang and Y. Shi, *AIP Advances*, 2014, **4**, 123004.

[17] B. C. Windom, W. Sawyer and D. W. Hahn, *Tribology Letters*, 2011, **3**, 301–310.

[18] M. Donarelli, S. Prezioso, F. Perrozzi, F. Bisti, M. Nardone, L. Giancaterini, C. Cantalini and L. Ottaviano, *Sensors and Actuators B: Chemical*, 2015, **207**, 602–613.

[19] N. Kang, H. P. Paudel, M. N. Leuenberger, L. Tetard and S. I. Khondaker, *The Journal of Physical Chemistry C*, 2014, **118**, 21258–21263.

[20] M. R. Islam, N. Kang, U. Bhanu, H. P. Paudel, M. Erementchouk, L. Tetard, M. N. Leuenberger and S. I. Khondaker, *Nanoscale*, 2014, **6**, 10033–10039.

[21] Y. Wang, Z. Ni, Z. Shen, H. Wang and Y. Wu, *Applied Physics Letters*, 2014, **92**, 043121.

[22] M. Buscema, G. A. Steele, H. S. van der Zant and A. Castellanos-Gomez, *Nano Research*, 2014, **7**, 561–571.

[23] S.-L. Li, H. Miyazaki, H. Song, H. Kuramochi, S. Nakaharai and K. Tsukagoshi, *ACS Nano*, 2012, **6**, 7381–7388.